Bull. Mater. Sci., Vol. 38, No. 4, August 2015, pp. 915–924. © Indian Academy of Sciences.

$NiCr_xFe_{2-x}O_4$ ferrite nanoparticles and their composites with polypyrrole: synthesis, characterization and magnetic properties

E H EL-GHAZZAWY[1,*] and S N ALAMRI[2]

[1]Physics Department, Faculty of Science, Tanta University, Tanta 31527, Egypt

[2]Physics Department, Faculty of Science, Taibah University, Madinah 30001, Saudi Arabia

Ms received 24 November 2014; accepted 20 February 2015

Abstract. **Nanocrystalline nickel chromium ferrite ($NiCr_xFe_{2-x}O_4$, $x = 0.1, 0.2$) have been prepared by the chemical co-precipitation method. Half of the samples have been sintered at 620°C and the other at 1175°C. Then polypyrrole (PPy)–$NiCr_xFe_{2-x}O_4$ composites have been synthesized by polymerization of pyrrole monomer in the presence of $NiCr_xFe_{2-x}O_4$ nanoparticles. The structure, morphology and magnetic properties of the samples have been characterized by X-ray diffraction (XRD), scanning electron microscopy (SEM), transmission electron microscopy (TEM) and Fourier transform infrared (FT-IR) spectroscopy and vibrating sample magnetometer. Also, the initial magnetic permeability measurements as functions of temperature and frequency have been performed. The XRD and FT-IR studies have confirmed the well crystalline phase of ferrite nanoparticles, and the presence of amorphous PPy in the composite samples. The SEM and TEM images have obviously clarified the coating of ferrite nanoparticles by PPy in the composite samples. The hysteresis loop of the samples has proved that the samples are soft magnetic material because of their low coercivity.**

Keywords. **Nanoparticles; ferrites; polypyrrole; composites; characterization; magnetic properties.**

1. Introduction

Magnetic–polymer composite materials gained increased technological importance because of the synthesis of new materials with combination of different functions and characteristics of organic and inorganic materials. Moreover, different inorganic materials including carbon nanotubes, metals and nano-sheets have been also investigated in polymer matrices.[1]

However, spinel ferrites had been intensively investigated for their important applications in transformer cores, antenna rods, inductors, magnetic bulk cores, magnetic fluids, microwave absorbers, magnetic drug delivery, medical diagnostics,[2] circulators, phase shifters, isolators, switches and tunable filters.[3] The crystallographic, electrical and magnetic properties of ferrites substantially depend on the conditions of preparation.[4]

Nickel ferrite ($NiFe_2O_4$) has become one of the important materials for decades, due to its unique electrical and magnetic properties that lead to extended technological applications.[5] $NiFe_2O_4$ is an inverted spinel with Ni^{2+} ions occupying almost half of the octahedral (B) sublattice. A small amount (5%) may be directed to the tetrahedral (A) sites under thermal equilibrium conditions.[6] The effect of substitution of Fe^{3+} by Cr^{3+} in $NiFe_2O_4$ has attracted a lot of attention where many authors had reported that X-ray and neutron diffraction results showed that Cr^{3+} always attempts to go to the octahedral sites in contrast to Fe^{3+} which is found at both sites.[7]

Bearing in mind that Cr^{3+} (3 μB) has a weaker magnetic moment than Fe^{3+} (5 μB), the partial replacement of Fe^{3+} by Cr^{3+} ion is expected to cause magnetic failure,[8] i.e., a decrease in saturation magnetization and coercivity of the sample.[9]

Moreover, the systems based on nanoparticles have been intensively studied both theoretically and practically due to their electric, dielectric and magnetic properties that are sensibly different from those of the bulk materials and their possible applications in various fields.[10]

On the other hand, conducting polymers are attractive materials, as they involve a wide range of functions and applications from insulators to metals.[11] It is well known that many physical and (electro) chemical properties of synthesized polypyrrole (PPy) are dependent on the dopant ion used. A lot of research works have proved the effect of the nature and size of the dopant on the PPy properties.[12]

Thus the conducting polymers have various practical applications, such as antistatic coatings, electromagnetic interference shielding,[13] field effect transistors, solar cells, electro-chromic devices, electronic circuits,[14] light-emitting diodes (LEDs[11]), supercapacitors and sensitive electrodes.[12] It is important to mention that PPy film has been used as protective coating layer for Ti–Al–V alloys which are used as orthopaedic devices.[15]

*Author for correspondence (enas7777777@gmail.com)

Large investigations have focused on developing synthetic methods for the preparation of nano-composites of electroactive polymers with noble metals or metal oxides.[16] Both polyaniline (PANI) and PPy are probably the most widely studied conducting polymers due to their good stability in air, high conductivity and reversible process between oxidation and reduction state. They are a new class of 'conductors' for electromagnetic shielding and microwave absorbing, which show a number of advantages over traditional granular materials.[17]

Soft magnetic ferrites with higher saturation magnetization, higher electrical resistivity and lower eddy current losses have been widely used in microwave devices such as isolators, circulators, phase shifters and gyrators. Thus composites formed from conducting polymer (PANI or PPy) and magnetic ferrite can be used as EMI shielding materials and have good shielding effectiveness for various electromagnetic sources.[18]

Li *et al*[19] have synthesized $ZnFe_2O_4$/PPy core–shell nanoparticles, and they found that $ZnFe_2O_4$/PPy core–shell nanoparticles exhibit excellent microwave absorption performance than $ZnFe_2O_4$ nanoparticles. Li *et al*[20] have prepared flake-like PPy/$SrFe_{12}O_{19}$ composites. It was found that the comprehensive magnetic property for the flocs-like $SrFe_{12}O_{19}$ was superior to the sphericity-like $SrFe_{12}O_{19}$ for the excellent magnetic aeolotropism of the flocs-like $SrFe_{12}O_{19}$. Lee *et al*[21] have prepared core–shell structure of $Mn_{1-x}Zn_xFe_2O_4$/PANI nano-composites. They have found that composite materials have stronger absorption for microwave between 3.5 and 6.5 GHz than that of pure spinel ferrites $MnFe_2O_4$

The aim of the present work is to obtain $NiCr_xFe_{2-x}O_4$ nanoparticles coated with PPy and study their structure, morphology and magnetic properties.

2. Experimental

2.1 *Preparation of $NiCr_xFe_{2-x}O_4$ nanoparticles*

$NiCr_xFe_{2-x}O_4$ ultra-fine particles with ($x = 0.1, 0.2$) were prepared by co-precipitating aqueous solutions of $NiCl_2{\cdot}6H_2O$, $CrCl_3{\cdot}6H_2O$ and $FeCl_3{\cdot}6H_2O$ by adding NaOH solution drop wise to the mixture solution under constant stirring until its pH value reaches 11.5. Then the solution was heated and maintained at about 90°C for 2 h under continuous stirring. The precipitate was thoroughly washed by distilled water, dried at 80°C and ground by an agate mortar to obtain ultrafine powder. One half of the obtained powder was sintered at 620°C, and the second half at 1175°C.

2.2 *Preparation of PPy–$NiCr_xFe_{2-x}O_4$ composites*

Four composite samples of PPy–$NiCr_xFe_{2-x}O_4$ ($x = 0.1, 0.2$, sintered at 620 and 1175°C) were prepared by polymerization of pyrrole monomers (using $FeCl_3{\cdot}6H_2O$ as an oxidizing agent) in the presence of $NiCr_xFe_{2-x}O_4$ nanoparticles; where 3 g of $NiCr_xFe_{2-x}O_4$ nanoparticles was suspended in a 50 ml of 0.1 M HCl solution and stirred for 30 min to get well dispersed suspension. Two millilitres of pyrrole monomer was added to the suspension and stirred for 30 min too. $FeCl_3{\cdot}6H_2O$ was dissolved in 50 ml of distilled water and this solution was added drop wise to the suspension mixture under a constant stirring. The polymerization was allowed to proceed for 2 h at room temperature. The composites were obtained by filtering and washing the suspension with distilled water, and dried at 80°C for 4 h.

3. Characterization

The powder samples were characterized by using a Shimadzu XRD-6000 X-ray diffractometer, using Cu K_α radiation ($\lambda = 1.5418$ Å) and the IR spectra in the range from 200 to 4000 cm^{-1} were recorded at room temperature using the infrared spectrometer (FT-IR spectrometer Tensor 27). The morphology of the samples was studied using a transmission electron microscope (JEOL JEM-100SX TEM) and a scanning electron microscope (SEM) (Shimadzu Super scan SSX-550+ EDX).

The magnetization measurements were carried out at room temperature up to maximum field of 20 kG, by using vibrating sample magnetometer (VSM), model Lake Shore 7410. The relative initial magnetic permeability of the solenoid powder samples was determined, as a function of temperature (in the range of 305–683 K for pure ferrites and 305–423 K for composite samples), using a simple resonance circuit, where μ_r was calculated using the formula $\mu_r = L_s/L_0$[22] (where L_0 and L_s are the inductance of the solenoid in the resonance circuit without and with sample inside, respectively). Also the initial permeability was determined as a function of frequency in the range of 100 Hz–100 kHz at room temperature by using the lock-in amplifier (Stanford Research Systems SR 510).

4. Results and discussion

4.1 *X-ray diffraction (XRD)*

The XRD patterns of $NiCr_xFe_{2-x}O_4$ show the characteristic peaks of single-phase cubic spinel at (111), (220), (311), (222), (400), (422), (511), (440) and (533), as shown in figure 1. The crystallite size 'D' of the $NiCr_xFe_{2-x}O_4$ particles has been calculated by Scherrer's equation:[23]

$$D = 0.89\lambda/\beta\cos\theta,$$

where λ is the X-ray wavelength, β the full-width at halfmaxima (FWHM) of the XRD peak at the (311) plane and θ the Bragg angle. The calculated crystallite size values are listed in table 1. The values confirm the nano-size of $NiCr_xFe_{2-x}O_4$ particles (<100 nm). Also, the samples are observed to exhibit enhanced crystallinity and increased crystallite size with the increase on the sintering temperature.

Since each primitive unit cell of the spinel structure contains 8 molecules, the value of the X-ray density, D_X was determined according to the relation:[24,25]

$$D_X = 8M/Na^3,$$

where 'M' is the molecular weight of the sample, 'N' Avogadro's number ($= 6.0225 \times 10^{23}$ atom mol^{-1}) and 'a' the lattice constant calculated from the X-ray data.

From table 1, it is also observed that the lattice constant and the d-spacing slightly decrease with the increase in the Cr^{3+} content because Cr^{3+} ions have a strong site preference of B-sites that leads to the replacement of Fe^{3+} ions at octahedral sites. Since there is a difference between the ionic radii of Cr^{3+} (0.64 Å) and Fe^{3+} (0.67 Å) ions, the lattice shrinks and the lattice parameters are expected to decrease.[4,26] It is observed also that the lattice parameters slightly decrease (or we can say the X-ray density increases) with the increase in the sintering temperature; that is, because during the sintering process, the thermal energy generates a force that may drive the grain boundaries to grow at the expense of pores so shrinkage can occur, therefore the material becomes denser.[27]

The interionic distances (i.e., cation–anion distances at A-site (d_{AL}) and B-site (d_{BL}), together with the distance of closest anion–anion approach, tetrahedral edge, d_{AE}, and shared and unshared octahedral edges, d_{BE}, d_{BEU}) are calculated according to the following equations:[25,28,29]

$$d_{AL} = a\sqrt{3}(u - 0.25),$$
$$d_{BL} = a(3u^2 - 11/4u + 43/64)^{1/2},$$
$$d_{AE} = a\sqrt{2}(2u - 0.5),$$
$$d_{BE} = a\sqrt{2}(1 - 2u),$$
$$d_{BEU} = a(4u^2 - 3u + 11/16)^{1/2},$$

where u is the oxygen parameter ($u = 0.3811$ for $NiFe_2O_4$).[30] Also the distances L_A and L_B between the magnetic ions at A-sites and B-sites (the jump length or hopping length), respectively, can be obtained where $L_A = a\sqrt{3}/4$, and $L_B = a\sqrt{2}/4$.[25,31] The calculated values are listed in table 2. It is clear that the values of d_{AL}, d_{BL}, d_{AE}, d_{BE}, d_{BEU} and the hopping length (L_A and L_B) decrease with the increase in the Cr^{3+} ion content. This is due to the replacement of larger radii ions (Fe^{3+}) by smaller radii ions (Cr^{3+}) in octahedral sites as mentioned above.[25,32]

XRD studies of the PPy–$NiCr_xFe_{2-x}O_4$ composite samples show that the PPy powders are amorphous in nature, as shown in figure 2. A broad peak was observed at about $2\theta \approx 26.5°$ along with the sharp peaks of the polycrystalline

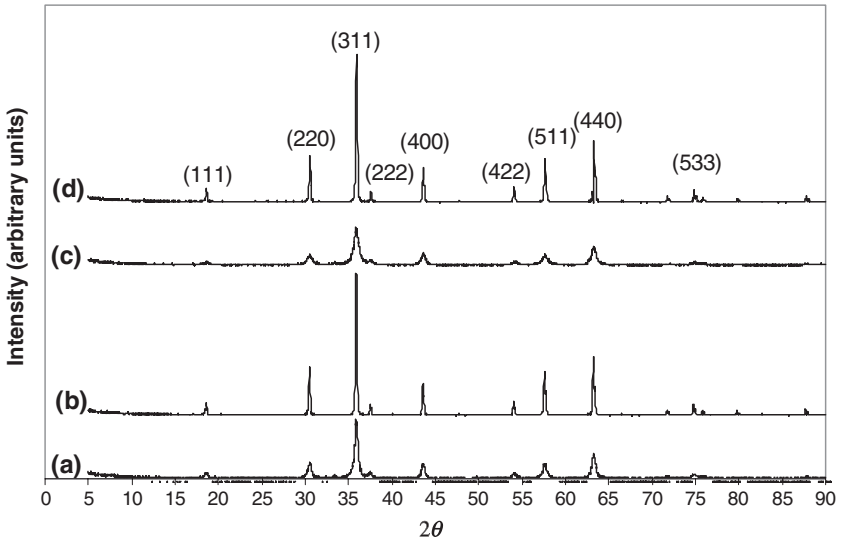

Figure 1. XRD. $NiCr_{0.1}Fe_{1.9}O_4$ sintered at (**a**) 620 and (**b**) 1175°C. $NiCr_{0.2}Fe_{1.8}O_4$ sintered at (**c**) 620 and (**d**) 1175°C.

Table 1. Values of lattice constant, X-ray density, crystallite size estimated from XRD and particle size estimated from TEM of $NiCr_xFe_{2-x}O_4$ samples.

Sample	Sintering temperature (°C)	Crystallite size (nm) XRD	Lattice constant (Å)	d-Spacing at (311) (A°)	XRD theoretical density	Particle size (nm) TEM
$NiCr_{0.1}Fe_{1.9}O_4$	620	19.70	8.2897 ± 0.01	2.4994	5.425	20.62
$NiCr_{0.1}Fe_{1.9}O_4$	1175	50.98	8.2892 ± 0.01	2.4993	5.426	49.15
$NiCr_{0.2}Fe_{1.8}O_4$	620	12.83	8.2894 ± 0.01	2.4993	5.448	19.75
$NiCr_{0.2}Fe_{1.8}O_4$	1175	51.88	8.2805 ± 0.01	2.4966	5.465	52.7

Table 2. Bond length of A-sites d_{AL} and B-sites d_{BL}, the tetrahedral edge d_{AE}, the shared and unshared octahedral edges, d_{BE} and d_{BEU} and the hopping length at A-site L_A and at B-site L_B for $NiCr_xFe_{2-x}O_4$ samples.

Sample	Sintering temperature (°C)	d_{AL} (Å)	d_{BL} (Å)	d_{AE} (Å)	d_{BE} (Å)	d_{BEU} (Å)	L_A (Å)	L_B (Å)
$NiCr_{0.1}Fe_{1.9}O_4$	620	1.8827	2.02312	3.0738	2.7878	2.9326	3.5894	2.9308
$NiCr_{0.1}Fe_{1.9}O_4$	1175	1.8822	2.023	3.0736	2.7876	2.9324	3.5892	2.9306
$NiCr_{0.2}Fe_{1.8}O_4$	620	1.8823	2.02305	3.0737	2.7877	2.9325	3.5893	2.9307
$NiCr_{0.2}Fe_{1.8}O_4$	1175	1.8803	2.02088	3.0704	2.7847	2.9293	3.5854	2.9275

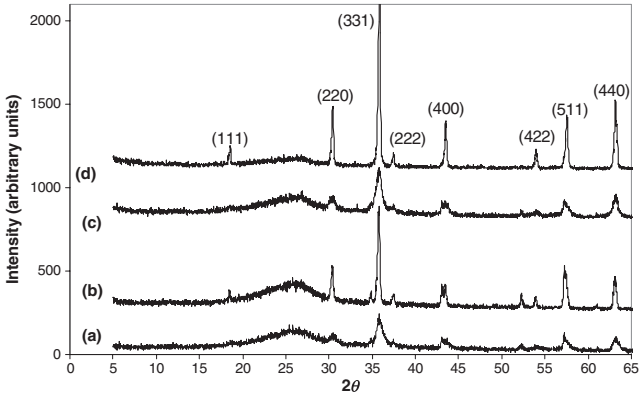

Figure 2. XRD. PPy–$NiCr_{0.1}Fe_{1.9}O_4$ composite prepared by ferrite sintered at (**a**) 620 and (**b**) 1175°C. PPy–$NiCr_{0.2}Fe_{1.8}O_4$ composite prepared by ferrite sintered at (**c**) 620 and (**d**) 1175°C.

ferrites. The broad peaks are characteristic of amorphous PPy and they are due to the scattering from PPy chains.[33] Such a broad peak usually indicates short-range arrangement of chains.[34]

4.2 *Morphology*

Figure 3 shows the SEM images of $NiCr_xFe_{2-x}O_4$ nanoparticle samples; these images clearly indicate that the distribution of the grains is homogeneous, consisting of well-crystalline grains.

On the other hand, the SEM images of PPy/ferrite composites (figure 4) reveal that the PPy is deposited on the surface of $NiCr_xFe_{2-x}O_4$ nanoparticles.

Figure 5 shows the TEM images of the $NiCr_xFe_{2-x}O_4$. From these images, it can be concluded that the co-precipitation method yield spherical or elliptical nanoparticles, with very small diameters, which is consistent with the XRD results estimated by the Scherrer formula, the particle size values estimated from TEM are listed in table 1. A tremendous change in the morphology of the composites has been observed after coating the $NiCr_xFe_{2-x}O_4$ nanoparticles by PPy as shown in figure 6. It is clearly seen that the coating by PPy has induced agglomeration. Moreover, the two phases constituting the composite are shown; where the darker colour regions may be attributed to $NiCr_xFe_{2-x}O_4$ and the grey regions may contain higher proportions of PPy.

4.3 *FT-IR spectra*

The room temperature FT-IR spectra of $NiCr_xFe_{2-x}O_4$ and PPy/ $NiCr_xFe_{2-x}O_4$ composites are shown in figures 7 and 8, respectively.

Generally, in the range 1000–300 cm^{-1}, the FT-IR bands of solids are usually assigned to vibration of inorganic ions in the crystal lattice.[35] The FT-IR spectra of $NiCr_xFe_{2-x}O_4$ show two strong absorption bands (ν_1) in the range of 590–607 cm^{-1} and (ν_2) in the range of 390–430 cm^{-1} as shown in figure 7. These two different bond vibrations are due to the difference in the distance between ions in both octahedral and tetrahedral sublattice sites.[36,37] The vibrational frequencies of the IR bands corresponding to tetrahedral and octahedral sites are given in table 3. It is observed that the bands ν_1 and ν_2 shift towards higher energy with increasing Cr^{3+} ions substitution for Fe^{3+} ions. This may be due to the reduction in the size of the unit cell.[38] The FT-IR spectra of the samples show prominent bands at about 3400 and 1600 cm^{-1} which are attributed to the stretching modes and H–O–H bending vibration of H_2O molecule.[35,39]

Figure 8 shows the FT-IR spectra of composite samples. It is observed that the two strong absorption bands of ferrites (ν_1 and ν_2) have disappeared. This may be due to the predominance of the PPy bands in the composite samples; where the bands around 1547 cm^{-1} (2,5-substituted pyrrole) and 1452 cm^{-1} are usually ascribed to the anti-symmetrical and symmetrical vibration bands of the pyrrole ring, respectively.[17] While the bands at about 1305 and 1042 cm^{-1} may correspond to C–H band in-plane deformation vibration[17,40] and the broad band at 1177 cm^{-1} may be assigned for N–C stretching band.[40] Finally, the peaks at 913 and 790 cm^{-1} may be related to the out-of-plane stretching vibration of C–H bond.[41]

4.4 *Magnetic properties*

4.4a *Hysteresis loop*: Figures 9 and 10 show the hysteresis loop of the $NiCr_xFe_{2-x}O_4$ and $NiCr_xFe_{2-x}O_4$/PPy samples, respectively. The samples presented very narrow hysteresis curves, indicating that their behaviour was that of soft magnetic materials.[17]

It is observed that the saturation magnetization (M_s) increases with the increase in the sintering temperature for ferrites and composite samples, that is due to the increase in grain size of ferrite nanoparticles[42,43] by decreasing the

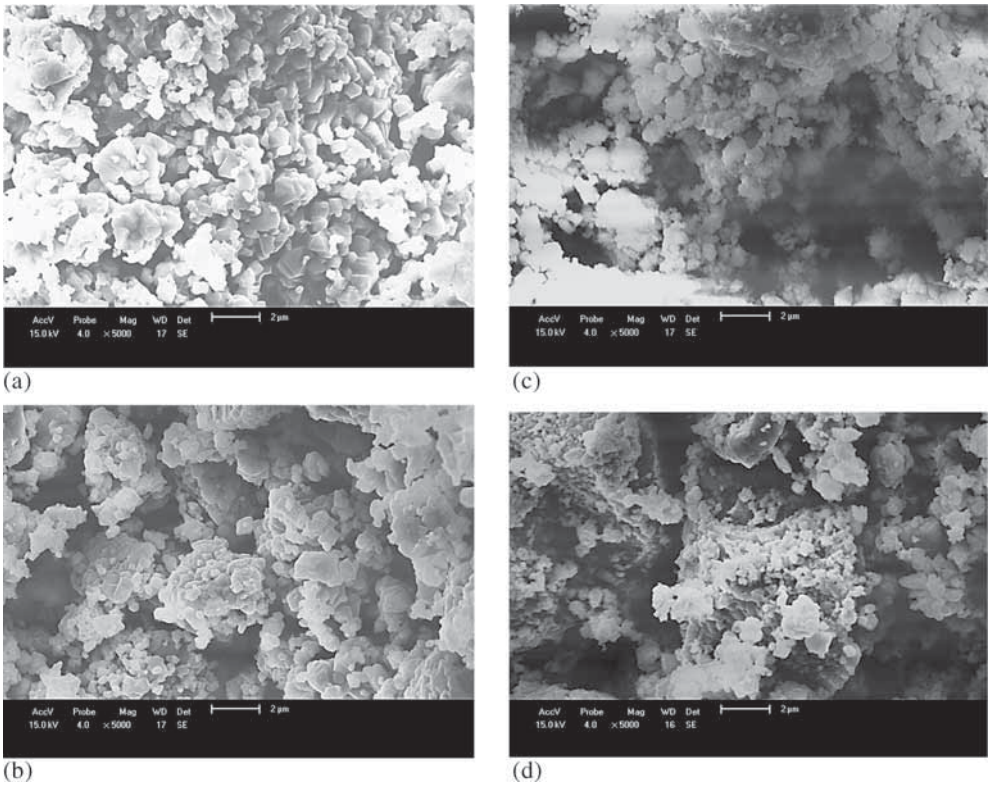

Figure 3. SEM. $NiCr_{0.1}Fe_{1.9}O_4$ sintered at (**a**) 620 and (**b**) 1175°C. $NiCr_{0.2}Fe_{1.8}O_4$ sintered at (**c**) 620 and (**d**) 1175°C.

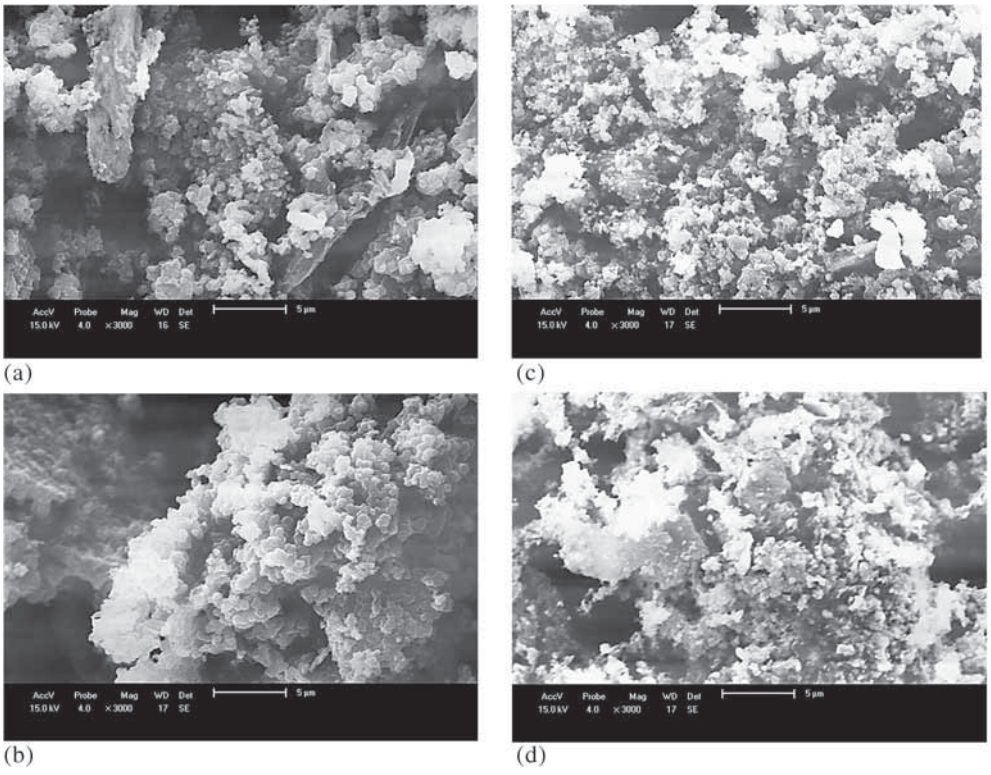

Figure 4. SEM. PPy–$NiCr_{0.1}Fe_{1.9}O_4$ composite prepared by ferrite sintered at (**a**) 620 and (**b**) 1175°C. PPy–$NiCr_{0.2}Fe_{1.8}O_4$ composite prepared by ferrite sintered at (**c**) 620 and (**d**) 1175°C.

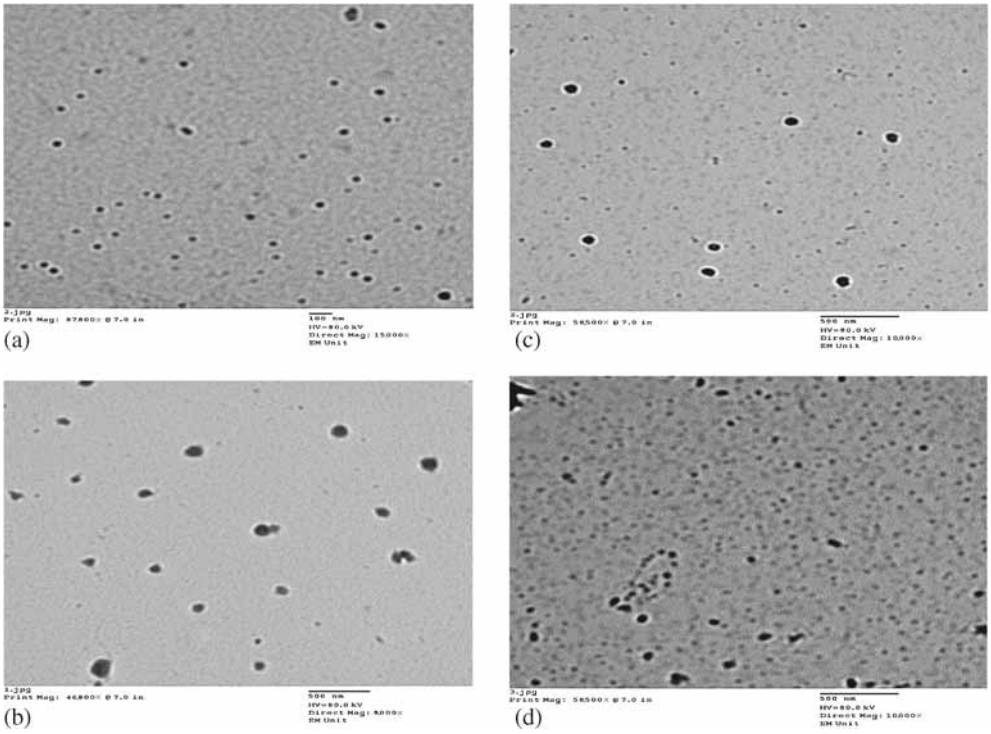

Figure 5. TEM. $NiCr_{0.1}Fe_{1.9}O_4$ sintered at (**a**) 620 and (**b**) 1175°C. $NiCr_{0.2}Fe_{1.8}O_4$ sintered at (**c**) 620 and (**d**) 1175°C.

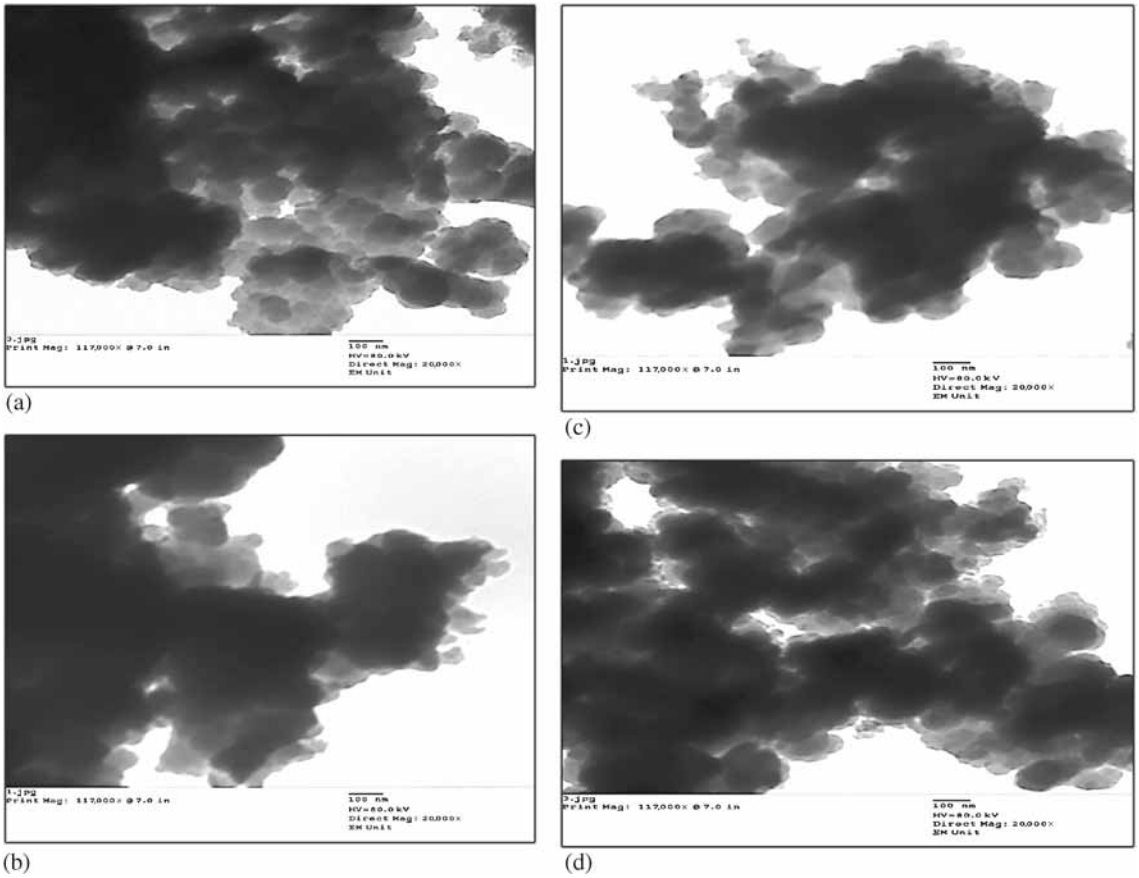

Figure 6. TEM. PPy–$NiCr_{0.1}Fe_{1.9}O_4$ composite prepared by ferrite sintered at (**a**) 620 and (**b**) 1175°C. PPy–$NiCr_{0.2}Fe_{1.8}O_4$ composite prepared by ferrite sintered at (**c**) 620 and (**d**) 1175°C.

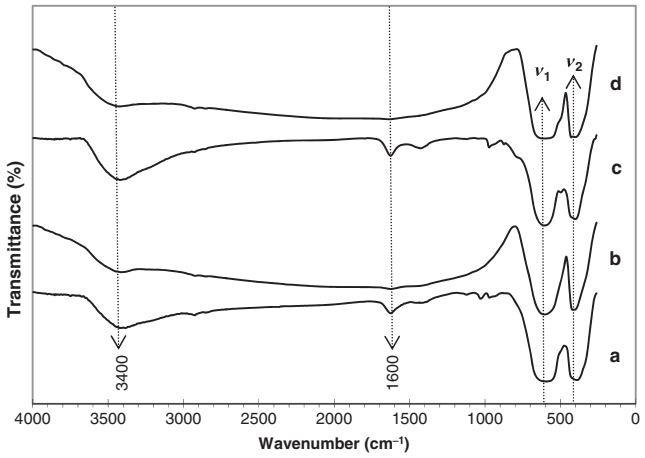

Figure 7. FT-IR. $NiCr_{0.1}Fe_{1.9}O_4$ sintered at (**a**) 620 and (**b**) 1175°C. $NiCr_{0.2}Fe_{1.8}O_4$ sintered at (**c**) 620 and (**d**) 1175°C.

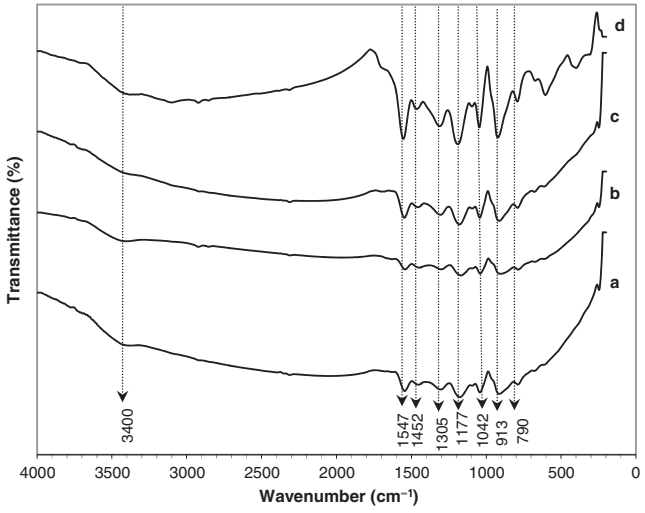

Figure 8. FT-IR. PPy–$NiCr_{0.1}Fe_{1.9}O_4$ composite prepared by ferrite sintered at (**a**) 620 and (**b**) 1175°C. PPy–$NiCr_{0.2}Fe_{1.8}O_4$ composite prepared by ferrite sintered at (**c**) 620 and (**d**) 1175°C.

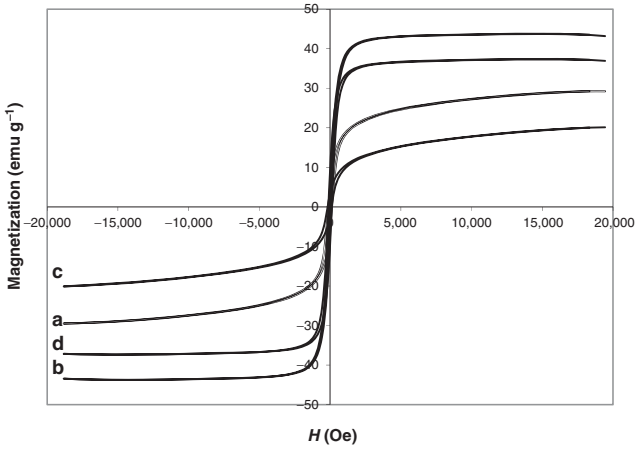

Figure 9. Magnetic hysteresis loop. $NiCr_{0.1}Fe_{1.9}O_4$ sintered at (**a**) 620 and (**b**) 1175°C. $NiCr_{0.2}Fe_{1.8}O_4$ sintered at (**c**) 620 and (**d**) 1175°C.

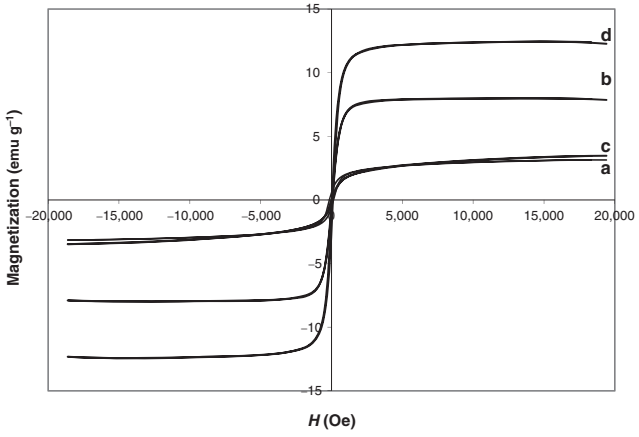

Figure 10. Magnetic hysteresis loop. PPy–$NiCr_{0.1}Fe_{1.9}O_4$ composite prepared by ferrite sintered at (**a**) 620 and (**b**) 1175°C. PPy–$NiCr_{0.2}Fe_{1.8}O_4$ composite prepared by ferrite sintered at (**c**) 620 and (**d**) 1175°C.

Table 3. Positions of IR absorption bands (ν_1, ν_2) of $NiCr_xFe_{2-x}O_4$ samples.

Sample	Sintering temperature (°C)	Wavenumber of absorption bands (ν) cm^{-1}	
		ν_1	ν_2
$NiCr_{0.1}Fe_{1.9}O_4$	620	590.2	389.60
$NiCr_{0.1}Fe_{1.9}O_4$	1175	605.6	420.47
$NiCr_{0.2}Fe_{1.8}O_4$	620	605.6	401.18
$NiCr_{0.2}Fe_{1.8}O_4$	1175	607.56	428.20

Table 4. Values of saturation magnetization M_s (emu g^{-1}) and the coercive field H_c (Oe) of the samples.

Sample	Sintering temperature (°C)	M_s (emu g^{-1})	H_c (G)
$NiCr_{0.1}Fe_{1.9}O_4$	620	29	127
$NiCr_{0.1}Fe_{1.9}O_4$	1175	43	48.5
$NiCr_{0.2}Fe_{1.8}O_4$	620	20.1	70
$NiCr_{0.2}Fe_{1.8}O_4$	1175	37	53.5
$NiCr_{0.1}Fe_{1.9}O_4$/PPy	620	3.1	140
$NiCr_{0.1}Fe_{1.9}O_4$/PPy	1175	7.9	57
$NiCr_{0.2}Fe_{1.8}O_4$/PPy	620	3.4	75.2
$NiCr_{0.2}Fe_{1.8}O_4$/PPy	1175	12.4	76.2

number of pores which cut the magnetic circuits between the grains[44] as displayed in table 4.

It is also noticed that the saturation magnetization in composite samples is lower than that of pure ferrite that is due to the contribution of nonmagnetic PPy coating layer to total magnetization.[18] It is known that PPy can separate the magnetic particles, which causes the transformation of co-linear

ferrimagnetic order of ferrite into non-co-linear arrangement and disruption of the ferrimagnetic order.[17]

While the values of H_c decrease with the increase in the sintering temperature because larger grains consist of large number of domain walls. So the magnetization/demagnetization due to domain wall movement which requires lower energy compared to that required for domain rotation will prevail.[45] While, the coercivity (H_c) values of composites are higher than that of pure ferrites because the PPy coating of ferrite particles increases the surface anisotropy of the composites.[19] In this study, Cr^{3+} ions are considered to be paramagnetic and do not contribute to the sublattice magnetization.[46] Hence from the hysteresis curves, it is observed that the saturation magnetization decreases with the increase in the chromium content because of the dilution of the magnetic moment of B-sublattice which weakens the A–B super-exchange interaction.[47]

The presence of Cr^{3+} ions in Ni ferrites resulted in a decrease of saturation magnetization and coercivity. These characteristics of soft ferrites are desirable for their utility in transformers and motor cores to minimize the energy dissipation with the alternating fields associated with AC electrical applications.[48]

It is also noticed that, the addition of chromium reduces the coercive field and softens the material, so these materials may be used in high-frequency transformers.[17]

4.4b *The initial permeability*: The initial permeability is considered to be an important magnetic property to study the quality of soft ferrites.[49]

Figures 11 and 12 show the variation of initial permeability with temperature for the $NiCr_xFe_{2-x}O_4$ and $NiCr_x$

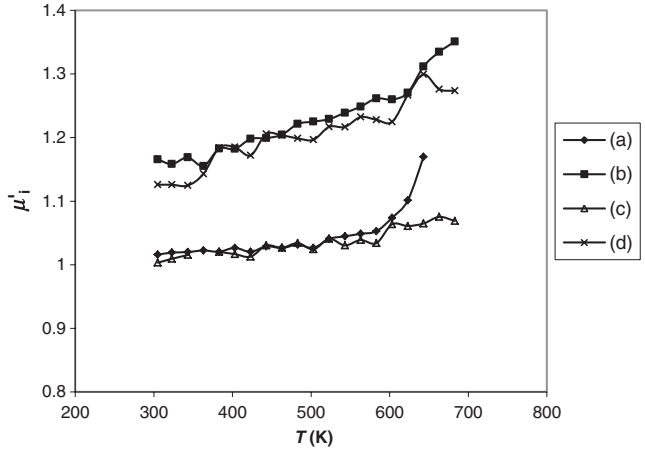

Figure 11. Variation of initial permeability with temperature. $NiCr_{0.1}Fe_{1.9}O_4$ sintered at (**a**) 620 and (**b**) 1175°C. $NiCr_{0.2}Fe_{1.8}O_4$ sintered at (**c**) 620 and (**d**) 1175°C.

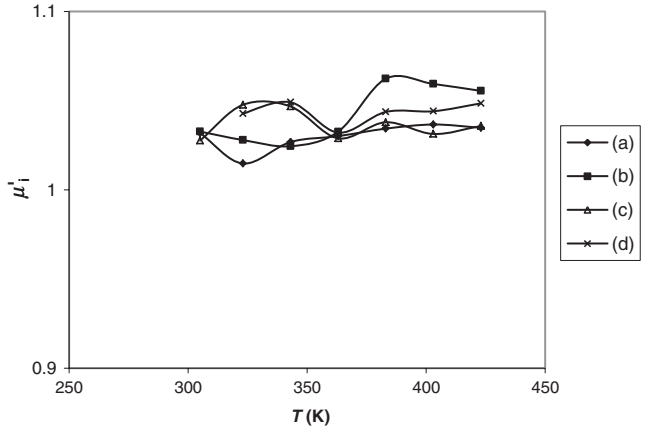

Figure 12. Variation of initial permeability with temperature. PPy–$NiCr_{0.1}Fe_{1.9}O_4$ composite prepared by ferrite sintered at (**a**) 620 and (**b**) 1175°C. PPy–$NiCr_{0.2}Fe_{1.8}O_4$ composite prepared by ferrite sintered at (**c**) 620 and (**d**) 1175°C.

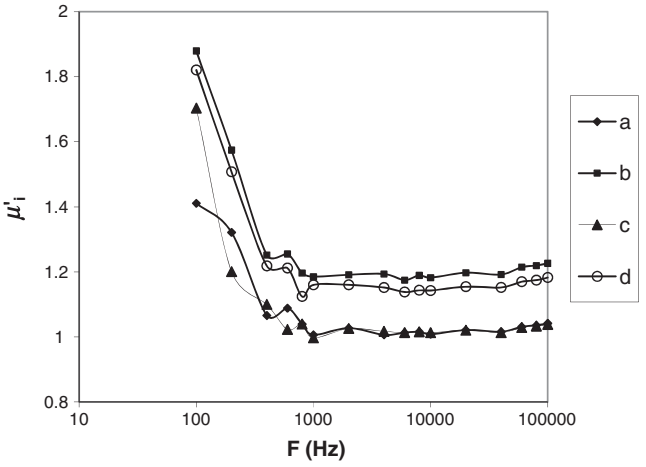

Figure 13. Variation of initial permeability with frequency. $NiCr_{0.1}Fe_{1.9}O_4$ sintered at (**a**) 620 and (**b**) 1175°C. $NiCr_{0.2}Fe_{1.8}O_4$ sintered at (**c**) 620 and (**d**) 1175°C.

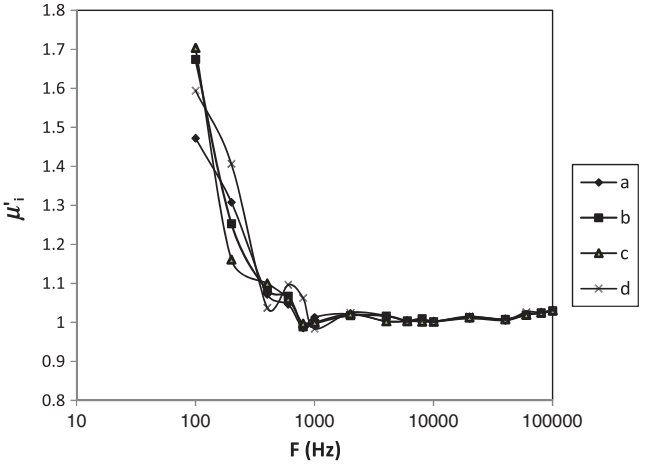

Figure 14. Variation of initial permeability with frequency. PPy–$NiCr_{0.1}Fe_{1.9}O_4$ composite prepared by ferrite sintered at (**a**) 620 and (**b**) 1175°C. PPy–$NiCr_{0.2}Fe_{1.8}O_4$ composite prepared by ferrite sintered at (**c**) 620 and (**d**) 1175°C.

$Fe_{2-x}O_4$/PPy samples, respectively. It can be seen that the initial permeability increases slightly with temperature. Above 600 K, the permeability increases fairly rapidly in ferrite samples especially in $NiCr_{0.1}Fe_{0.9}O_4$ samples (figure 11) that may indicate a growth in grain size by heating. In addition, this may be due to the decrease of the anisotropy field with the increase in temperature, which leads to an increase in the permeability.[50] It is also observed that the high sintering temperature samples have higher permeability values because the number of pores decreases. Also, the increase in the sintering temperature results in a decrease in the magnetic anisotropy by decreasing the internal stresses and crystal anisotropy which facilitates the movement of the domain walls.[51] It is also observed that the initial permeability decreases with the increase in the paramagnetic chromium ions.

The effect of PPy is clearly shown in figure 12. It is seen that the permeability of the composites is lower than that of $NiCr_xFe_{2-x}O_4$ ferrite nano-particles as expected due to the diamagnetic PPy contribution to the total magnetization as mentioned above.

Curie temperature of $NiCr_xFe_{2-x}O_4$ is relatively high ($T_c = 845.7$ K at $x = 0.0$ and $T_c = 804.49$ K at $x = 0.2$) as discussed by other authors[52] so it is not observed in our temperature range.

The complex initial permeability can be expressed by the following relation:

$$\mu_i = \mu_i' - j\mu_i'',$$

μ_i' is the real part of initial permeability, known as initial permeability and μ_i'' the imaginary part of initial permeability also known as permeability loss.

The frequency variation of initial permeability showed dispersion at low frequency (figures 13 and 14) and becomes nearly constant, maintaining a low value, at higher frequencies. At low frequencies, changes of the magnetization direction occur by the domain wall motion, so that a domain oriented in the direction of the applied field grows at the expense of its neighbours which are oriented in different directions. At higher frequencies, the domain wall is unable to move sufficiently rapidly to follow the alternating field so the permeability decreases.[53]

It is seen that for all compositions the initial permeability is independent of frequency from 1 to 100 kHz (at constant room temperature).

It is worth noting that the values of the initial permeability measured using two different techniques (a simple resonance circuit and lock in amplifier) are nearly the same, this confirms that the results are correct.

5. Conclusions

$NiCr_xFe_{2-x}O_4$ nanoparticles could be successfully synthesized via the co-precipitation method. X-ray and FT-IR study confirm the formation of single-phase spinel structure. The inter-ionic distances decrease with the increase in the Cr^{3+} content. PPy/$NiCr_xFe_{2-x}O_4$ composites could be successfully synthesized by polymerization of PPy in the presence of $NiCr_xFe_{2-x}O_4$ nanoparticles. XRD patterns of the composite samples show that the PPy has definitely an amorphous nature. The morphology studies confirm the nanoscale diameter of $NiCr_xFe_{2-x}O_4$ particles. The magnetic parameters such as saturation magnetization, coercivity and permeability of the samples depend on the composition and sintering temperature. The effect of Cr^{3+} ions in the samples is to decrease the magnetic parameters that makes the samples are candidates to be used in transformers, motor cores and high-frequency applications. The samples $NiCr_xFe_{2-x}O_4$/PPy are shown to be superparamagnetic, which allows them to serve as ideal candidates for biomedical applications, such as nucleic acid extraction, cancer diagnosis and treatment, biosensors and drug delivery. The electric properties are currently under investigation to be published in the near future.

References

1. Xie Y, Hong X, Gao Y, Li M, Liu J, Wang J and Lu J 2012 *J. Synth. Met.* **162** 677
2. Wahba A M and Mohamed M B 2014 *J. Ceram. Int.* **40** 6127
3. Mallégol S, Quéffélec P, Le Floc'h M and Gelin P 2003 *J. IEEE Trans. Magn.* **39** 2003
4. Hashim M, Alimuddin Kumar S, Shirsath S E, Kotnala R K, Shah J and Kumar R 2013 *J. Ceram. Int.* **39** 1807
5. Khan M A, Islam M, Iqbal M A, Ahmad M, Din M F, Murtaza G, Ahmad I and Warsi M F 2014 *J. Ceram. Int.* **40** 3571
6. Dionne G F 2009 *Magnetic oxides* (USA: Springer Science)
7. Gismelseed A M and Yousif A A 2005 *J. Phys. B* **370** 215
8. Birajdar A A, Shirsath S E, Kadam R H, Patange S M, Mane D R and Shitre A R 2012 *J. Ceram. Int.* **38** 2963
9. Köseoğlu Y, Oleiwi M I O, Yilgin R and Kocbay A N 2012 *J. Ceram. Int.* **38** 6671
10. Gul I H, Ahmed W and Maqsood A 2008 *J. Magn. Magn. Mater.* **320** 270
11. Jiang J, Chen C, Ai L, Li L and Liu H 2009 *J. Mater. Lett.* **63** 560
12. Hallik A, Alumaa A, Kurig H, Jänes A, Lust E and Tamm J 2007 *J. Synth. Met.* **157** 1085
13. Yavuz O, Ram M, Aldissi M, Poddar P and Srikanth H 2005 *J. Synth. Met.* **151** 211
14. Carquigny S, Segut O, Lakard B, Lallemand F and Fievet P 2008 *J. Synth. Met.* **158** 453
15. Kumar A M and Rajendran N 2013 *J. Ceram. Int.* **39** 5639
16. Mahmoudian M R, Alias Basirun W J, Woi P M, Baradaran S and Sookhakian M 2014 *J. Ceram. Int.* **40** 9265
17. Li L, Xiang C, Liang X and Hao B 2010 *J. Synth. Met.* **160** 28
18. Liangchao L, Haizhen Q, Yuping W, Jing J and Feng X 2008 *J. Rare Earths* **26** 558
19. Li Y, Yi R, Yan A, Deng L, Zhou K and Liu X 2009 *J. Solid State Sci.* **11** 1319
20. Li Q, Zhang C, Wang Y and Li B 2009 *J. Synth. Met.* **159** 2029
21. Lee S, Chen Y, Ho C, Chang C and Hong Y 2007 *J. Mater. Sci. Eng. B* **143** 1

22. Saafan S A, Meaz T M and El-Ghazzawy E H 2011 *J. Magn. Magn. Mater.* **323** 1517
23. Alam J, Riaz U and Ahmad S 2007 *J. Magn. Magn. Mater.* **314** 93
24. Attia S A 2006 *J. Solids* **29** 329
25. Dhiman R L, Taneja S P and Reddy V R 2008 *J. Adv. Condens. Matter Phys.* **2008** Article ID 703479, 7 doi: 10.1155/2008/703479
26. El-Sayed A M 2002 *J. Ceram. Int.* **28** 651
27. Islam R, Rahman M O, Hakim M A, Saha D K, Saiduzzaman Noor S and Al-Mamun M 2012 *J. Mater. Sci. Appl.* **3** 326
28. Pandit A A, More S S, Dorik R G and Jadhav K M 2003 *J. Bull. Mater. Sci.* **26** 517
29. Rana M U, Ul-Islam M and Abbas T 2002 *J. Appl. Sci.* **2** 1110
30. Wohlfarth E P 1982 *Ferromagnetic materials* (Amsterdam: North-Holland Publication Co.)
31. Dhiman R L, Taneja S P and Reddy V R 2008 *J. Adv. Condens. Matter Phys.* Article ID 839536, 7 doi: 10.1155/2008/839536
32. Kawade V B, Bichile G K and Jadhav K M 2000 *J. Mater. Lett.* **42** 33
33. Waghuley S A, Yenorkar S M, Yawale S S and Yawale S P 2008 *J. Sens. Actuators* **128** 366
34. Chitte H K, Bhat N V, Walunj V E and Shinde G N 2011 *J. Sens. Technol.* **1** 47
35. Priyadharsini P, Pradeep A, Rao P S and Chandrasekaran G 2009 *J. Mater. Chem. Phys.* **116** 207
36. Ghasemi A and Vinia M M 2014 *J. Ceram. Int.* **40** 2825
37. Kaiser M 2009 *J. Alloys Compd.* **468** 15
38. Amer M A, Meaz T M, Ata-Allah S, Aboul-Enein S and Abd-El-Hamid M O 2005 *J. Solids* **28** 275
39. Skoog D A 1985 *Principles of instrumental analysis* (USA: Saunders Golden Sunburst Series)
40. Vishnuvardhan T K, Kulkarni V R, Basavaraja C and Raghavendra S C 2006 *J. Bull. Mater. Sci.* **29** 77
41. Wang Y, Li L, Jiang J, Liu H, Qiu H and Xu F 2008 *J. Reactive Funct. Polym.* **68** 1587
42. Singhal S, Bhukal S, Singh J, Chandra K and Bansal S 2011 *J. Nanotechnol.* doi: 10.1155/2011/930243
43. Rao B P and Caltun O F 2006 *J. Optoelectron. Adv. Mater.* **8** 991
44. Fawzi A S 2011 *J. Adv. Appl. Sci. Res.* **2** 577
45. Verma A, Goel T C, Mendiratta R G and Kishan P 2000 *J. Magn. Magn. Mater.* **208** 13
46. Fu Y P, Hung D S and Yao Y D 2009 *J. Ceram. Int.* **35** 2179
47. Kumar A M, Varma M C, Choudary G, Rao K S, Rao K H and Gopalakrishna G 2010 *J. Optoelectron. Adv. Mater.* **12** 2386
48. Raghasudha M, Ravinder D and Veerasomaiah P 2013 *J. Nanostruct. Chem.* **3** 63
49. Mangalaraja R V, Lee S T, Ananthakumar S, Manohar P and Camurri C P 2008 *J. Mater. Sci. Eng. A* **476** 234
50. Sattar A A, El-Sayed H M, Agami W R and Ghani A A 2007 *Am. J. Appl. Sci.* **4** 89
51. Verma A, Goel T C and Mendiratta R G 2000 *J. Magn. Magn. Mater.* **210** 274
52. Lee S H, Yoon S J, Lee G J, Kim H S, Yo C H, Ahn K, Lee D H and Kim K H 1999 *J. Mater. Chem. Phys.* **61** 147
53. Soibam I, Phanjoubam S, Sharma H B, Sarma H N K and Prakash C 2009 *J. Phys. B* **404** 3839